PB89-207245

Narrow-Gap Point-to-Plane Corona with High Velocity Flows

(U.S.) Environmental Protection Agency
Research Triangle Park, NC

1988

U.S. Department of Commerce
National Technical Information Service
NTIS

AEERL-P-491

TECHNICAL REPORT DATA
(Please read Instructions on the reverse before comple

1. REPORT NO. EPA/600/J-88/311	2.	3 PB89-207245
4. TITLE AND SUBTITLE Narrow-gap Point-to-plane Corona with High Velocity Flows		5. REPORT DATE 6. PERFORMING ORGANIZATION CODE
7. AUTHOR(S) Toshiaki Yamamoto, Phil A. Lawless (RTI), and Leslie E. Sparks (EPA)		8. PERFORMING ORGANIZATION REPORT NO.
9. PERFORMING ORGANIZATION NAME AND ADDRESS Research Triangle Institute P.O. Box 12194 Research Triangle Park, North Carolina 27709		10. PROGRAM ELEMENT NO. 11. CONTRACT/GRANT NO. CR812281
12. SPONSORING AGENCY NAME AND ADDRESS EPA, Office of Research and Development Air and Energy Engineering Research Laboratory Research Triangle Park, NC 27711		13. TYPE OF REPORT AND PERIOD COVERED Journal article; 9/86-2/88 14. SPONSORING AGENCY CODE EPA/600/13

15. SUPPLEMENTARY NOTES AEERL project officer is Leslie E. Sparks, Mail Drop 54, 919/541-2458. IEEE Transactions of Industry Applications, 24:5, pp. 934-939, 9-10/88. Also Industry Applications Society Meeting, Denver, 9/28-10/2/86.

16. ABSTRACT The article discusses a mathematical model developed to describe a narrow-gap point-to-plane corona system used in the detoxification of chemical agents or their simulants, for which the degree of destruction depends on the strength of the electric field or electron energy. Narrow-gap electrodes are characterized by extremely high electron activity and the presence of positive and negative ions. The three-dimensional spatial distributions in the electron density and the electric field are of primary interest. The results address the potential problems of the corona device and help to provide for an optimum design.

17. KEY WORDS AND DOCUMENT ANALYSIS

a. DESCRIPTORS	b. IDENTIFIERS/OPEN ENDED TERMS	c. COSATI Field/Group
Pollution	Pollution Control	13B
Electric Corona	Stationary Sources	20C
Detoxification		06E
Mathematical Models		12A
Electrodes		09A

REPRODUCED BY
U.S. DEPARTMENT OF COMMERCE
NATIONAL TECHNICAL INFORMATION SERVICE
SPRINGFIELD, VA. 22161

18. DISTRIBUTION STATEMENT Release to Public	19. SECURITY CLASS *(This Report)* Unclassified	21. NO. OF PAGES 9
	20. SECURITY CLASS *(This page)* Unclassified	22. PRICE

EPA Form 2220-1 (9-73)

EPA/600/J-88/311

Narrow-Gap Point-to-Plane Corona with High Velocity Flows

TOSHIAKI YAMAMOTO, PHIL A. LAWLESS, AND LESLIE E. SPARKS

Abstract—**Corona discharge has been used in the detoxification of chemical agents or their simulants, for which the degree of destruction depends on the strength of the electric field or electron energy. To help clarify this process a mathematical model describing the narrow-gap point-to-plane corona system was developed. Narrow-gap electrodes are characterized by extremely high electron activity and the presence of positive and negative ions. The three-dimensional spatial distributions in the electron density and the electric field are of primary interest. The results address the potential problems of the corona device and help to provide for an optimum design.**

I. Introduction

CORONA discharge has been used in the detoxification of chemical agents or their simulants. Tests were made on the corona device, which consists of narrow-gap multiple point-to-plane geometry devices in which the gas passes through a corona discharge at high velocity (~100 m/s) [1]. Ozone is thought to be the primary agent in the gas destruction. Experiments have shown that more ozone can be generated with an increased current density (or voltage) and that increasing the gas velocity will increase the sparkover potential considerably. It is desirable, therefore, to operate the electrical potential at as high a level as possible. The experimental results showed that the average field and the average current per point were extremely high (18 kV/cm and 1.0 mA/point, respectively). The ozone generation rate was approximately 250 ppm/kW of corona power, and destruction efficiency was proportional to the ozone generation. However, the destruction efficiency was extremely poor (~15 percent) and was not additive with the number of corona points. It was further reduced by increasing the pin-to-plane distance.

For detoxification it is apparent that the discharge region is the area where useful reactions are most likely to occur. The highest electric fields and electron energies exist in this region, and it is expected that the radicals and excited atomic states have the greatest concentrations there. While investigating the point-to-plane corona, Kondo and Miyoshi [2] found that spectroscopic evidence estimated a temperature in excess of 1000°K near the point corona. It appears from a simple destruction efficiency model (no mixing in the transverse direction) that the active zones for either a high electron activity or a high temperature are in a very narrow confined region. Making optimal use of these factors requires a better understanding of the detailed electrical conditions in this region. This paper describes the modeling that calculates the electrical characteristics of corona discharge devices in varied corona discharge configurations.

Paper IUSD 86-81, approved by the Electrostatic Processes Committee of the IEEE Industry Applications Society for presentation at the 1986 Industry Applications Society Annual Meeting, Denver, CO, September 28–October 2. This work supported by the U.S. Environmental Protection Agency under cooperative agreement CR-812281-01-0. Manuscript released for publication February 24, 1988.

T. Yamamoto and P. A. Lawless are with the Research Triangle Institute, Center for Aerosol Technology, P.O. Box 12194, Research Triangle Park, NC 27709.

L. E. Sparks is with the Air and Energy Engineering Research Laboratory MD-61, U.S. Environmental Protection Agency, Research Triangle Park, NC 27711.

IEEE Log Number 8821469.

II. Modeling

Corona glow discharge has been studied for many years. Satisfactory theories about corona discharge outside the corona glow region have been developed through both numerical and analytical methods. Because of the complicated discharge physics, the knowledge of corona discharge within the glow region is more limited. The corona discharge device under study consists of a narrow-gap channel with a point-to-plate distance of 3.0 mm. Therefore the regions both inside and outside the glow corona are modeled.

We first modeled the Townsend avalanche mechanisms. Then we developed a narrow-gap three-dimensional ion flow model. The model will be completed when the spatial distributions of electrons and ions (as determined by the avalanche model) are incorporated into the three-dimensional corona model.

A. Townsend Electron Avalanche Modeling

Because the role of free electrons in the agent destruction process is still uncertain (although probably important), it is necessary to evaluate the electron concentration under various conditions and then correlate these values with the results of destruction tests. We approach the electron density question from a theoretical point of view, using the Townsend avalanche mechanism to describe the corona zone with its mix of electrons and positive and negative ions. This approach lets us vary the gas pressure and temperature, the spacing between the corona point and the ground plate, and the effects of gas composition. In return, electron and ion concentration profiles are produced.

The Townsend avalanche is a conceptual description of the electron multiplication process. The process begins with a free electron in a strong electric field. The electron gains enough energy between collisions and gas molecules to ionize one of them. This produces another electron and a positive ion. The two free electrons are then able to produce two more ionizations, and the process multiplies rapidly. The rate at which the ionizations occur is described by a derived gas parameter, the first Townsend coefficient. The first Townsend coefficient is the number of electrons produced per centimeter per initial electron.

NTIS is authorized to reproduce and sell this report. Permission for further reproduction must be obtained from the copyright owner.

© 1988 IEEE

The first Townsend coefficient has been determined experimentally for many gases as a function of electric field and gas density. It generally becomes larger as the electric field increases or the gas density decreases. In the electric field near a corona electrode, the first Townsend coefficient (gas gain coefficient) varies rapidly with position in relation to the surface of the electrode.

The Townsend avalanche can easily grow to enormous levels if there are no effects to offset its growth. One such effect is a rapid decrease in the electric field as the distance from a corona electrode increases. This effect is not sufficient to ensure a stable corona, however. Another offsetting effect is that free electrons become permanently attached to certain gas molecules. They then become negative ions and are removed from the avalanche process. A last limiting effect is the buildup of the ionic concentrations. The positive ions that remain behind the advancing electron front tend to retard the electrons, and the negative ions formed by attachment tend to repel later generations of electrons.

In air, the major attachment occurs with oxygen molecules. This attachment rate is also dependent on the electric field, though not as strongly as the gas gain. The attachment rate is described by the attachment coefficient, which is the number of electrons attached per centimeter per initial electron. Generally, the attachment rate goes up when the electric field goes down because the electrons spend more time in the neighborhood of attaching molecules.

The avalanche is calculated by integrating three differential equations:

$$dn_e = (\alpha - \eta) n_e dx \tag{1}$$

$$dn_p = (\alpha) n_e dx \tag{2}$$

$$dn_m = (-\eta) n_e dx \tag{3}$$

where n_e is the number of electrons at position x, n_p is the number of positive ions at position x, and n_m is the number of negative ions at position x. The coefficients, α and η, are evaluated according to the electric field at position x, which is derived from an expression for the electrostatic field for a needle-to-plane geometry.

This integration is performed by a predictor–corrector algorithm, with the step size varied to keep the increase in electron population within reasonable bounds for each step. Although the equations are coupled through the electron number, they are linear for low densities of positive and negative ions. When those densities become large, the electric field at position x is a function of both all the existing ion densities and the electrostatic field. This makes the equations very nonlinear.

Direct-current coronas develop over several generations of electron avalanches. A single avalanche cannot produce the observed currents at the observed voltages. There are good physical mechanisms for some of the positive ions to produce additional electrons from the surface of the corona point, leading to successive avalanches. We call these "new generations" because they develop from the prior avalanche's ionic production. The ions remain relatively stationary in space during the later generations, because the electrons move so rapidly that each avalanche is completed in the time it takes the positive ions to move a fraction of a millimeter. Thus the ions produced by successive generations are added to the ion concentrations already at a given position.

Over many generations, the ionic densities remain too small to influence the electric field very much. However, when a critical density is reached where the field near the corona point is strongly enhanced by the presence of the nearly positive ion cloud, one last avalanche produces so many ions and electrons that the prior cumulative total is small by comparison. It also causes the electric field to be reduced to zero or even reversed in direction by the ionic space charge near the corona point. (This is "quenching," a phenomenon commonly described in the corona literature.) Further corona avalanches cease until most of the space charge is removed at a relatively slow pace by the electric fields.

Spectroscopic measurements of coronas show the presence of very high temperatures, as much as 1000°K in the core of the corona zone. These high temperatures would be expected to reduce the gas density, increase the electron and ion diffusivity in the core, and probably modify the generation process substantially. By simulating a high-temperature profile in the corona, we have succeeded in achieving conditions where the positive space charge cannot reach the extreme values that cause quenching. The corona mechanism becomes effectively continuous, thus confirming experimental results that show a pulseless regime [2].

B. Three-Dimensional Electron Flow Model for Point-to-Plane Corona Discharge in a High-Velocity Flow

Outside the corona generation region, the combined electron and ion flows must be modeled. One crucial factor in the modeling is assuming that the flow of current away from the corona generation zone is caused by unattached electrons. Since the electron mobility has a value several hundred times greater than that of ions [3], most of the current will be carried by the unattached electrons for the narrow-gap configuration. For the first approximation, we considered the electrons as the only carrier of current. We performed a numerical simulation of the three-dimensional point-to-plane corona discharge. For the present, we assume that only the electrons are present at a constant time-averaged concentration and that they have a constant mobility.

The Maxwell equations and current continuity equations, coupled with high flow velocity, describe both the electric field and current density distributions:

$$\text{div } \vec{E} = \rho_e / \epsilon_0, \tag{4}$$

$$\text{div } \vec{J} = 0, \tag{5}$$

$$\vec{J} = \rho_e (b_e \vec{E} + \vec{U}_f), \tag{6}$$

$$\text{grad } V = -\vec{E} \tag{7}$$

where E = electric field, ϵ_0 = permittivity of the gas, ρ_e = electron space charge density, J = current density, U_f = gas velocity, b_e = electron mobility, V = electrical potential, and $\rightarrow$ represents vectors.

The current continuity equation (5), coupled with the

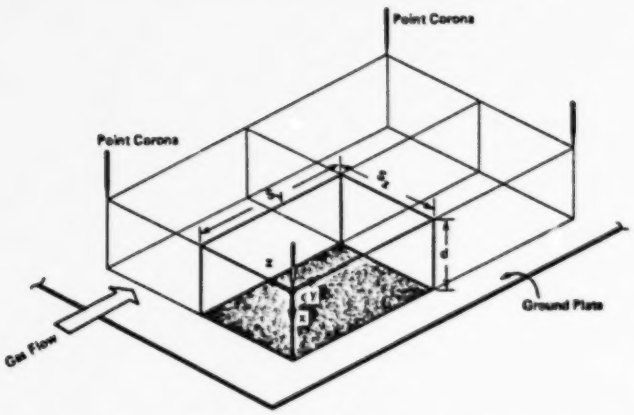

Fig. 1. Point-to-plane corona discharge geometry.

primary flow, can be modified as

$$\rho_e^2 = \epsilon_0 [\text{grad } \rho_e \cdot \text{grad } V - (\text{grad } \rho_e) \cdot \bar{U}_f / b_e]. \quad (8)$$

Both (4) and (8) are expressed as a finite difference scheme and are solved simultaneously. Fig. 1 describes the working domain in the point-to-plane geometry. A series of inner grid points (for the numerical simulation of a given differential equation and the coordinates x, y, z) is indicated in this figure. Since the electron velocity is much greater than the gas velocity, the second term in the right side of (8) can be neglected in the present analysis. Hence the symmetry conditions apply along the plane normal to the gas flow direction. The boundary conditions can be written as

$V = V_0$ (applied voltage) at the point,

$V = 0$ on the ground plate,

E_x, E_y, and $E_z = 0$ on the symmetry planes, and

$$I \text{ (calculated)} = I \text{ (measured)} \quad (9)$$

where E_x, E_y, and E_z = electric field in the x, y, and z directions, respectively, and I = total current. Because the computational methods solving the three-dimensional model are similar to those of Yamamoto and Sparks [4], this is omitted in this paper.

III. Results and Discussion

A. Townsend Electron Avalanche Modeling

The first point of interest is that the operating voltage of the device (for a given point-to-plane spacing) is determined primarily by the radius of the point tip. This is expected from observations of corona over the years, but has not been verified, especially for the narrow-gap devices. The magnitude of the onset voltage is changed only by a few hundred volts, with tip radii changing from 0.25 mm to 0.025 mm.

Figs. 2(a) and 2(b) show the distributions of ions and electrons as a function of the distance from the points for (a), the small radius electrode, and (b), the large radius electrode. The positive and negative concentration curves represent the true concentration, constant in time. The electron concentration curve represents the instantaneous concentration of an electron generation (or swarm) as it progresses from point to plane. Only a small volume of space would be occupied by the electrons at any one time.

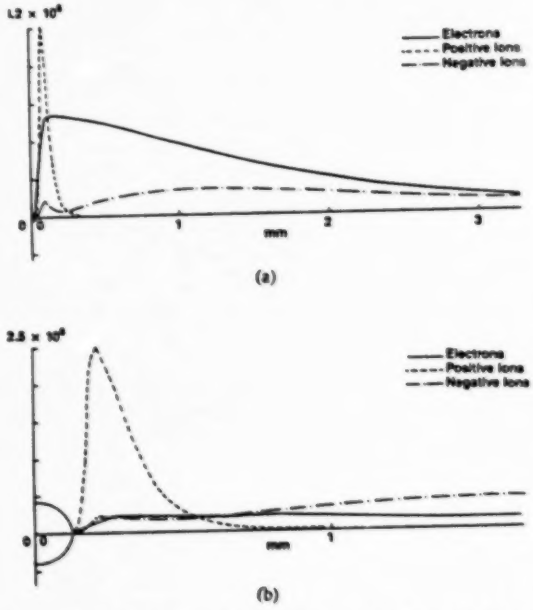

Fig. 2. Distributions of ions and electrons as function of position. (a) Small-radius electrode. (b) Large-radius electrode.

The larger radius tips also provide a somewhat more uniform free-electron concentration (from tip to plane). This is a consequence of the electric field configuration. The sharper the tip radius is, the higher the field near the tip. At the same time, it decays away from the tip more rapidly. For a fixed tip-to-plane distance, there is a critical radius above which the corona immediately develops into a sparking condition [5].

Although the avalanche model does not address questions of either the corona's stability or the effects of air flow through the corona zone, the behavior of the model (under different assumptions about the temperature profile) leads us to speculate about the flow's effect. Generally, the electrons

travel farther with higher core temperatures (because of the reduced gas density). The electrons also carry most of the current (because of their high mobility) and therefore contribute the most to the heating of the gas. It seems, therefore, that the corona instability is due to self-heating of the gas and that the cross-flow stabilizes the corona primarily by cooling the gas.

The avalanche model does show strong sensitivity toward the composition of the gas atmosphere in the electron attachment process. Since ionization in air occurs predominantly in the nitrogen and oxygen components, the first Townsend coefficient is not strongly affected by small additions of other gases. On the other hand, the attachment coefficient in air is relatively small so that additions of attaching gases can have a strong effect. Increasing the attachment coefficient by a factor of 10 restricts the corona to a small region near the tip and reduces the electron current considerably. Decreasing the attachment coefficient by a factor of 10 leads to a nearly uniform electron density from tip to plane and increases the current flow.

B. Three-Dimensional Electron Flow Modeling for the Point-to-Plane Configuration

The voltage of V_0 was 4200 V and a current density of 1.0 mA/needle was used for the numerical computation. The electrode-to-plate distance (d) was maintained at 3.0 mm, the point distance in the y direction (S_y) was maintained at 6.0 mm, and the point-to-plane spacings (S_z) were varied. The other variables involved were temperature of the gas, which was assumed to be 550°C, and the electron mobility, which was assumed to be 500 times greater than ion mobility (b_e = 0.447 m²/V/s). The grid points used for this computation were (7 × 10 × 10). The maximum error was within 5.3 percent when the grid points were doubled.

The results of this simulation consist primarily of computer graphics displays. These displays provide information on the three-dimensional electrical potential, electric field, and electron density distributions. Figs. 3(a) and 3(b) show the electric field in the x-component ($\bar{E}_x$) distribution, normalized by the average field $E_0 = V_0/d$ for d = 3 mm, S_z = 3 mm, S_y = 6 mm, and various y and z values. The values of electric field and electron density are quite high in the vicinity of the point corona, indicating very high electron energy activities. Increasing of S_z increases the value of $\bar{E}_x$ near the corona point in the y direction, but decreases in the y and z directions as approaching the ground plate. The effect of the electron space charge is rather small because of the higher electron mobility. Thus the electron space-charge distribution does not have an appreciable effect on either the potential or the electric field distributions.

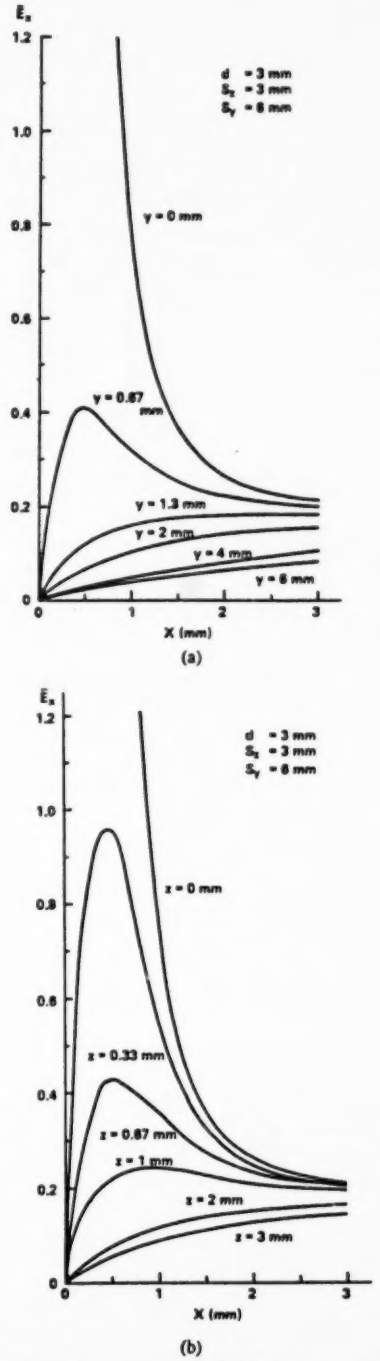

Fig. 3. Distributions of normalized electric field in x direction.

Since the product of electron density and electric field E_x (electron force density) is of primary interest, their contours in the y-z plane with various distances x from the plate are shown in Figs. 4(a)–4(d). Fig. 4(a) shows contours at the ground plate, level 7 ($x = d$), for S_z = 3.0 mm, S_y = 6.0 mm, and d = 3.0 mm. The contours represent 0.1, 0.3, 0.5, and one higher value of the maximum electron force density ($\rho_e E_x$) that occurs directly beneath the point corona. The 0.1 contours represent an absolute value of approximately 4.2 A/m².

Moving one-third of the distance toward the point corona, to level 5 ($x = 2d/3$), gives the electron force density distribution in Fig. 4(b). Figs. 4(c) and 4(d) are up further, levels 3 ($x = d/3$) and 2 ($x = d/6$). Note that the electron force densities are zero at level 1 ($x = 0$) except at the corona point. Integration of these four figures will give a three-

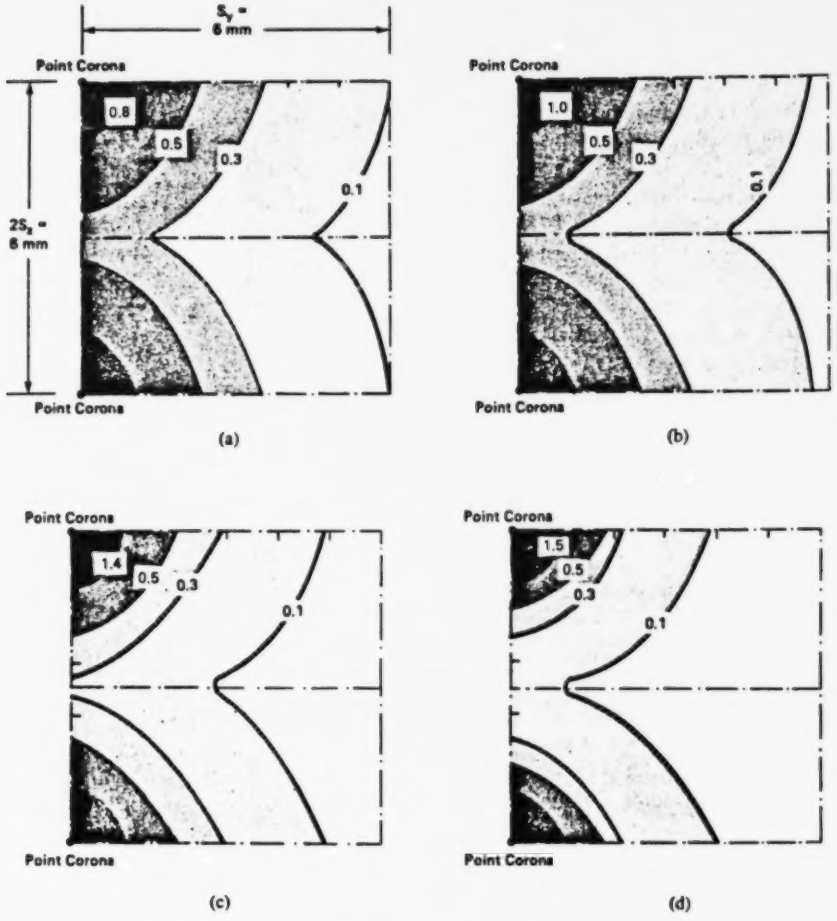

Fig. 4. Contours of electron force density distributions for narrow-point spacing (S_z = 3.0 mm). (a) Level 7 ($x = d$). (b) Level 5 ($x = 2d/3$). (c) Level 3 ($x = d/3$). (d) Level 2 ($x = d/6$).

dimensional view of the electron force density distributions obtained. Notice the regions of lower electron force density between the corona points. This is the region where the gas can escape reaction and, consequently, avoid chemical destruction.

Wide point space (S_z = 6.0 mm) yielded curves of similar shape as shown in Figs. 5(a)-5(d). Fig. 5(a) shows the contours of electron force density at level 7 ($x = d$). Figs. 5(b)-5(d) also show their distribution at levels 5 ($x = 2d/3$), 3 ($x = d/3$), and 2 ($x = d/6$), respectively. The maximum and normalized value was 3.5 A/m^2, which is 20 percent lower than the value for narrow spacing. Notice that the active energy region was further reduced by increasing the spacing. Although this active zone can be minimized by reducing the point-to-point distance, a considerable fraction of electron force density remains low.

IV. Conclusion

A mathematical model describing the narrow-gap point-to-plane corona system is being developed using a microcomputer. The model is menu-driven and flexible, allowing a variety of simulations to be run. The Townsend avalanche model gives ion and electron concentrations as a function of distance from the corona point. The results are sufficiently conclusive to show that few electrons will be found more than 3.0 mm from the corona point. Thus, if the electron concentration is an important factor in chemical reaction, then the 3.0-mm gap devices should work much better than devices with a larger gap.

The three-dimensional ion flow simulation showed that, although the low electron force region can be minimized by reducing the point spacing, there is still a considerable fraction of nonactive zones, resulting in electrical sneakage.

If high temperatures are significant contributors to the agent-destruction efficiency, then the model assumes, at present, that the diameter of the high-temperature zone is less than 1 mm. This is in accordance with both the magnified observations of the active region of the corona and the spectroscopic measurements of Kondo and Miyoshi [2].

In the future, the effect of both positive and negative ions, the gas velocity, and the field-dependent electron mobility will be incorporated for the corona modeling.

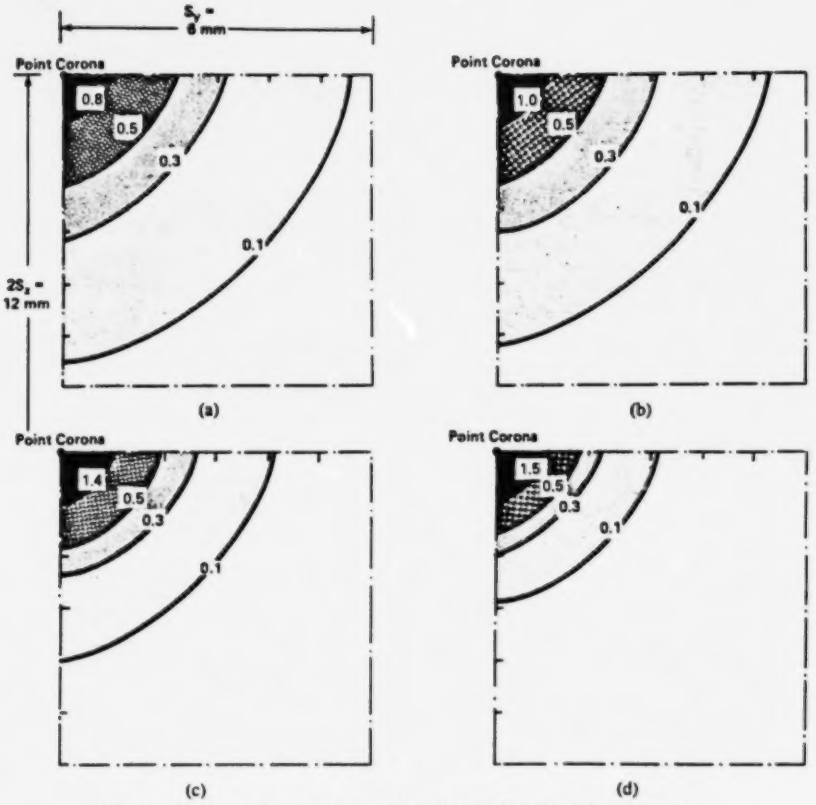

Fig. 5. Contours of electron force density distributions for wide-point space (S_x = 6.0 mm). (a) Level 7 ($x = d$). (b) Level 5 ($x = 2d/3$). (c) Level 3 ($x = d/3$). (d) Level 2 ($x = d/6$).

References

[1] P. M. Castle, I. E. Kanter, P. K. Lee, and L. E. Kline, "Corona glow detoxification study," Westinghouse Corporation, final report contract DAAA 09-82-C-5396, 1984.

[2] Y. Kondo and Y. Miyoshi, "Pulseless corona in negative point to plane gap," *Jap. J. of Appl. Phys.*, vol. 17, pp. 643–649, 1978.

[3] L. B. Loeb, *Basic Processes of Gaseous Electronics.* Berkeley, CA: University of California, 1961.

[4] T. Yamamoto and L. E. Sparks, "Numerical simulation of three-dimensional tuft corona and electrohydrodynamics," in *IEEE Trans. Ind. Appl.*, vol. IA-22, no. 5, pp. 880–885, Sept./Oct. 1986.

[5] F. W. Peek, Jr., *Dielectric Phenomena in High-Voltage Engineering.* New York/London: McGraw-Hill, 1929.

Toshiaki Yamamoto received the M.S. degree in energy engineering from the University of Illinois, Chicago, in 1972 and the Ph.D. degree in mechanical engineering from Ohio State University, Columbus, in 1979.

He is a Research Engineer in the chemical engineering unit of Research Triangle Institute (RTI), Research Triangle Park, NC, where he is involved various aspects of electrostatic precipitator technologies, indoor air pollution, and microcontamination control technology. Prior to joining RTI, he was an Adjunct Professor of mechanical engineering as well as a Research Engineer at the Denver Research Institute of the University of Denver.

Dr. Yamamoto is a member of Sigma Xi, ASME, IES, AAAR, IEJ, and JAAST and the author of numerous publications on particulate control technologies.

Phil A. Lawless received the Ph.D. degree in physics from Duke University in 1974.

That year, he joined the Research Triangle Institute, where he has worked on and led research in many fields. For the past ten years, he has worked on aerosol research projects, with particular emphasis on electrostatic precipitator (ESP) research. He has made significant contributions toward the development of mathematical models of the precipitation process, including prediction of the voltage-current characteristics of wire-plate precipitators.

Dr. Lawless is a member of the American Association for Aerosols Research and of the Electrostatic Processes Committee of the IEEE-IAS. He is the author of numerous publications on the modeling of ESPs.

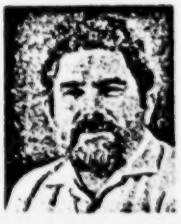

Leslie E. Sparks received the M.S. degree in chemical engineering and the Ph.D. degree in air resources engineering, both from the University of Washington, Seattle.

He joined the U.S. Environmental Protection Agency (EPA) in 1971, where he has managed projects to develop more efficient and cost-effective controls for particulate-matter emissions. His specialty has been advancing the state of the art in electrostatic precipitator (ESP) technology. He has recently managed development of low-cost multistage ESPs, an advanced computer model for ESPs—designed for use on personal computers—and the combined particulate and SO_x removal (E-SO_x) process. He is the author of numerous publications on control of particulate-matter emissions.

Dr. Sparks is a member of the American Institute of Chemical Engineers, the American Association for the Advancement of Science, the Air Quality Coalition, and the Air Pollution Control Association.

NOTICE

This document has been reviewed in accordance with U.S. Environmental Protection Agency policy and approved for publication. Mention of trade names or commercial products does not constitute endorsement or recommendation for use.

This article documents research that was conducted under the auspices of the U.S. Environmental Protection Agency (USEPA). As an arm of the government, the USEPA has a paid up, non-exclusive, irrevocable, worldwide license to reproduce, prepare derivative works, and distribute to the public all of the material contained herein, and to grant others acting on its behalf the right to do so. The USEPA grants to the National Technical Information Service, Department of Commerce, the right to act as its agent in the distribution of this material.